Organic Electronics 11 (2010) 41–49

Contents lists available at ScienceDirect

Organic Electronics

journal homepage: www.elsevier.com/locate/orgel

Synthesis, crystal structure and photo- and electro-luminescence of the coumarin derivatives with benzotriazole moiety

Tianzhi Yu [a,*], Peng Zhang [a,b], Yuling Zhao [b], Hui Zhang [a], Jing Meng [a], Duowang Fan [a], Lili Chen [c], Yongqing Qiu [c]

[a] Key Laboratory of Opto-Electronic Technology and Intelligent Control (Lanzhou Jiaotong University), Ministry of Education, Lanzhou 730070, China
[b] School of Chemical and Biological Engineering, Lanzhou Jiaotong University, Lanzhou 730070, China
[c] Institute of Functional Material Chemistry, Faculty of Chemistry, Northeast Normal University, Changchun 130024, China

ARTICLE INFO

Article history:
Received 15 July 2009
Received in revised form 22 September 2009
Accepted 23 September 2009
Available online 9 October 2009

Keywords:
Synthesis
Coumarin derivative
Benzotriazole
Photo- and electroluminescence

ABSTRACT

Two new coumarin derivatives containing an electron-transporting moiety (benzotriazole), 7-*N*,*N*-diethylamino-3-(benzotriazol-1-yl)coumarin (DABTC-1) and 7-*N*,*N*-diethylamino-3-(benzotriazol-2-yl)coumarin (DABTC-2), were synthesized and characterized by element analysis, ^{1}H NMR, FT-IR and UV–vis absorption spectra. Their structures were determined by X-ray crystallography single crystal analysis. The photoluminescent behaviors of the compounds in both solution and solid states were observed, they exhibit strong blue and blue–green emissions under ultraviolet light excitation, respectively. The energy levels of the HOMO and LUMO of the compounds have been calculated with density functional theory (DFT) and time-dependent density functional theory (TD-DFT) at B3LYP/6-31G(d) level. The electroluminescent devices with the compounds as the emitters were fabricated.

1. Introduction

Organic light-emitting diodes (OLEDs) based on organic materials are known to be highly efficient and are capable of producing a wide range of colors, which have attracted considerable interest and constitute a rapidly developing field due to their potential use in the development of energy-efficient, low-cost, full-color, flat-panel displays and other emissive products [1–4].

Coumarin derivatives exhibit not only excellent biological and medical activities [5], but also have super thermal stability and outstanding optical properties including an extended spectral response, high quantum yields, superior photostability. Optical applications of these compounds, such as laser dyes, nonlinear optical chromophores, fluorescent whiteners, fluorescent probes, polymer science, optical recording and solar energy collectors, have been widely investigated [6–12]. More important, coumarin dyes were used as blue, green and red dopants in organic light-emitting diodes (OLEDs) [13–15]. However, coumarin dyes are easily self-quenched in high concentration due to the intermolecular interactions and aggregations, so as the light-emitting materials they are always doped in the host materials at appropriate concentration to fabricate OLEDs with reasonable, luminant efficiency [16–19]. 7-*N*,*N*-diethylaminocoumarin dyes substituted at 3-position with an electron-withdrawing group are a typical class of D-A structure molecules and exhibit strong fluorescence [20–22]. So some of these coumarin derivatives have been used in the fabrication of OLEDs through doping in polymer matrix or Alq_3 thin layer as guest-emitting materials [23].

Recently, we synthesized two new coumarin derivatives, 7-*N*,*N*-diethylamino-3-(benzotriazol-1-yl)coumarin (DABTC-1) and 7-*N*,*N*-diethylamino-3-(benzotriazol-2-yl)-coumarin (DABTC-2), using the Knoevenagel type of condensation reaction (Scheme 1). The compounds exhibit strong blue and blue-green emissions under ultraviolet light excitation, respectively. Here, the photophysical properties of the compounds in diluted chloroform

* Corresponding author. Tel.: +86 931 4956935; fax: +86 931 4938756.
E-mail address: Ytz823@hotmail.com (T. Yu).

1566-1199/$ - see front matter © 2009 Elsevier B.V. All rights reserved.
doi:10.1016/j.orgel.2009.09.023

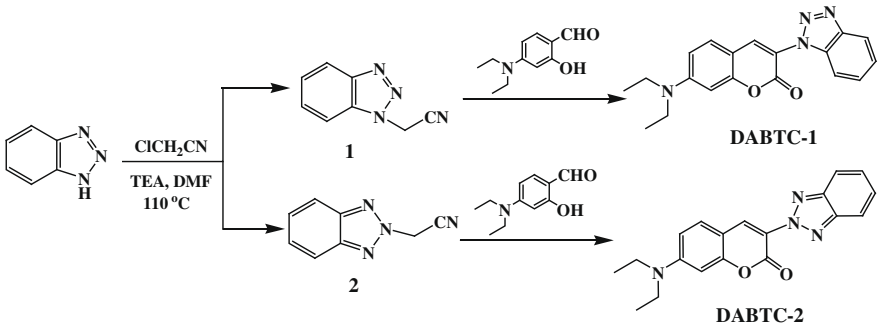

Scheme 1. Synthetic routes of 7-*N*,*N*-diethylamino-3-(benzotriazol-1-yl)coumarin and 7-*N*,*N*-diethylamino-3-(benzotriazol-2-yl)coumarin.

solutions and thin films were investigated in detail. We fabricated the electroluminescence devices by vacuum vapor-deposited film with doped with the compounds as emission materials and investigated the electroluminescent properties.

2. Experimental details

2.1. Materials and methods

4-(*N*,*N*′-diethylamino) salicylaldehyde from Zhejiang Huadee Dyestuff Chemical Co. Ltd. (China) was recrystallized from ethanol. 1H-benzotriazole (BTA) from Aldrich was used without further purification. Triethylamine, piperidine and chloroacetonitrile were analytical grade reagents from Tanjin Fuchen Chemical Reagent Factory. 4,4′-bis(9-carbazolyl) biphenyl (CBP), 2-(4-biphenylyl)-5-(4-tert-butylphenyl)-1,3,4-oxadiazole (Bu-PBD), 4,4′,4″-tris-N-naphthyl-*N*-phenylamino-triphenylamine (2-TNATA) and *N*,*N*′-bis-(naphthyl)-*N*,*N*′-diphenyl-1,1′-biphenyl-4,4′-diamine (NPB) were purchased from Electro-Light Technology Corp., Beijing. The other solvents were analytical grade reagents.

IR spectra (400–4000 cm^{-1}) were measured on a Shimadzu IRPrestige-21 FT-IR spectrophotometer. ^1H NMR spectra were obtained on Unity Varian-500 MHz. C, H, and N analyses were obtained using an Elemental Vario-EL automatic elemental analysis instrument. Melting points were measured by using an X-4 microscopic melting point apparatus made in Beijing Taike Instrument Limited Company, and the thermometer was uncorrected. UV–vis absorption and photoluminescent spectra were recorded on a Shimadzu UV-2550 spectrometer and on a Perkin–Elmer LS-55 spectrometer, respectively. The electroluminescent spectra were measured on a Hitachi MPF-4 spectrometer.

2.2. Synthesis and characterization of 7-N,N-diethylamino-3-(benzotriazol-1-yl)coumarin (DABTC-1) and 7-N,N-diethylamino-3-(benzotriazol-2-yl)coumarin (DABTC-2)

The synthetic routes were shown in scheme 1.

2.2.1. 2-(1H-benzotriazol-1-yl)acetonitrile (**1**) and 2-(1H-benzotriazol-2-yl)acetonitrile (**2**)

The intermediates **1** and **2** were synthesized by condensation of 1*H*-benzotriazole with chloroacetonitrile in DMF at reflux in the presence of triethylamine according to the method reported by Sanna et al. [24].

2.2.2. 7-N,N-diethylamino-3-(benzotriazol-1-yl)coumarin (DABTC-1)

1.93 g (10 mmol) of 4-(*N*,*N*′-diethylamino) salicylaldehyde, 1.67 g (10.6 mmol) 2-(1*H*-benzotriazol-1-yl)acetonitrile (**1**) were dissolved in 16 mL of anhydrous alcohol and treated with piperidine (0.6 mL). The reaction mixture was refluxed with stirring for 49 h, treated with HCl (3.5%), and boiled for 5 h. After the reaction was finished, the resulting mixture was poured into 50 mL of water and extracted with dichloromethane (3 × 50 mL). The organic phase was washed with water (2 × 50 mL) and dried over anhydrous $MgSO_4$. After filtering, the filtrate was evaporated to dryness under reduced pressure. The crude was purified by chromatography on silica gel using ethyl acetate/petroleum ether (1:6, v/v) as the eluent to give 7-*N*,*N*-diethylamino-3-(benzotriazol-1-yl)coumarin (DABTC-1) (1.12 g, 33.5%). m.p. 164–165 °C. 1H NMR: (500 MHz, $CDCl_3$, δ, ppm): 8.116 (d, J = 4.8 Hz, 1H, Aryl-H), 8.049 (s, 1H, 4-H), 7.619–7.594 (m, 1H, Aryl-H), 7.565–7.554 (m, 1H, Aryl-H), 7.540–7.516 (m, 1H, Aryl-H), 7.434–7.388 (m, 1H, Aryl-H), 6.678 (d, J = 7.9 Hz, 1H, Aryl-H), 6.608 (s, 1H, Aryl-H), 3.503–3.451 (m, 4H, $-CH_2-$), 1.261 (t, J = 6.4 Hz, 6H, $-CH_3$). IR (KBr pellet cm^{-1}): 3060 (Aryl-CH), 2971, 2929, 2891 (Alkyl-CH), 1728 (C=O, lactone), 1628 (C=C), 1590, 1524, 1421, 1250, 1121, 752. Anal. Calc. for $C_{19}H_{18}O_2N_4$ (%): C, 68.25; H, 5.43; N, 16.76. Found: C, 68.53; H, 5.57; N, 16.84.

2.2.3. 7-N,N-diethylamino-3-(benzotriazol-2-yl)coumarin (DABTC-2)

0.49 g (2.53 mmol) of 4-(*N*,*N*′-diethylamino) salicylaldehyde, 0.40 g (2.53 mmol) 2-(1*H*-benzotriazol-2-yl)acetonitrile (**2**) were dissolved in 12 mL of absolute alcohol, and then piperidine (0.2 mL) was dropped under ice bath. The mixture was stirred for 12 h at room temperature, treated with HCl (3.5%) and boiled for 5 h. After the reaction was finished, the resulting mixture was poured into 20 mL of water and extracted with dichloromethane (3 × 20 mL). The organic phase was washed with water and dried over anhydrous $MgSO_4$. After filtering, the filtrate was evaporated to dryness under reduced pressure. The crude was purified by chromatography on silica gel using ethyl acetate/petroleum ether (1:6, v/v) as the eluent to give 7-

N,*N*-diethylamino-3-(benzotriazol-2-yl)coumarin (DABTC-2) (0.63 g, 74.8%). m.p. 156–158 °C. ^{1}H NMR: (500 MHz, $CDCl_3$, δ, ppm): 8.280 (s, 1H, 4-H), 7.954 (d, J = 4.8 Hz, 2H, Aryl-H), 7.441–7.264 (m, 3H, Aryl-H), 6.682 (d, J = 8 Hz, 1H, Aryl-H), 6.608 (s, 1H, Aryl-H), 3.484–3.440 (m, 4H, $-CH_2-$), 1.255 (t, J = 5.2 Hz, 6H, $-CH_3$). IR (KBr pellet cm^{-1}): 3067 (Aryl-CH), 2975, 2925, 2871 (Alkyl-CH), 1731 (C=O, lactone), 1624 (C=C), 1573, 1517, 1421, 1233, 1125, 745. Anal. Calc. for $C_{19}H_{18}O_2N_4$ (%): C, 68.25; H, 5.43; N, 16.76. Found: C, 68.51; H, 5.72; N, 16.37.

2.3. Crystallography

Suitable crystals of DABTC-1 and DABTC-2 were obtained by evaporation of ethyl acetate solutions, respectively. The diffraction data were collected with a Bruker Smart Apex CCD area detector using a graphite-monochromated Mo Kα radiation (λ = 0.71073 Å) at 20 °C. The structures of DABTC-1 and DABTC-2 were solved by using the program SHELXL and Fourier difference techniques, and refined by full-matrix least-squares method on F^2. All hydrogen atoms were added theoretically. The crystals and experimental data of DABTC-1 and DABTC-2 are shown in Table S1. The selected bond lengths and bond angles of DABTC-1 and DABTC-2 are listed in Tables S2 and S3, respectively.

2.4. Quantum chemical calculations

The structure of DABTC-1 and DABTC-2 were optimized by semiempirical density functional theory (DFT) using a B3LYP/6-31G (d) basis set. The structural energies of DABTC-1 and DABTC-2 were calculated at B3LYP/6-31G(d) levels. The structure optimization and energy calculations were performed with the GAUSSIAN 98 program.

2.5. OLEDs fabrication

The multilayer OLEDs were fabricated by vacuum-deposition method. ITO-coated glass with a sheet resistance $R_\square \sim 20\ \Omega/\square$ was cut into 3 cm × 3 cm plates and etched in dilute hydrochloric acid for 20 min. Then the ITO substrates were routinely cleaned by ultrasonic treatment in solvents and then cleaned by exposure to an UV–ozone ambient. All organic layers were sequentially deposited without breaking vacuum (2×10^{-4} Pa). Thermal deposition rates for organic materials, LiF and Al were ~2 Å/s, ~1 Å/s and 10 Å/s, respectively. The active area of the devices was 12 mm^2. The EL spectra were measured on a Hitachi MPF-4 fluorescence spectrometer. The characterization of brightness–current–voltage (B–I–V) were measured with a 3645 DC power supply combined with a 1980A spot photometer and were recorded simultaneously. All measurements were done in the air at room temperature without any encapsulation.

3. Results and discussion

3.1. X-ray crystal structures of DABTC-1 and DABTC-2

The crystal structures and packing diagrams of DABTC-1 and DABTC-2 are given in Figs. 1–4, respectively. The crystal data and experimental details are shown in Table S1. The selected bond lengths and bond angles of DABTC-1 and DABTC-2 are listed in Tables S2 and S3, respectively.

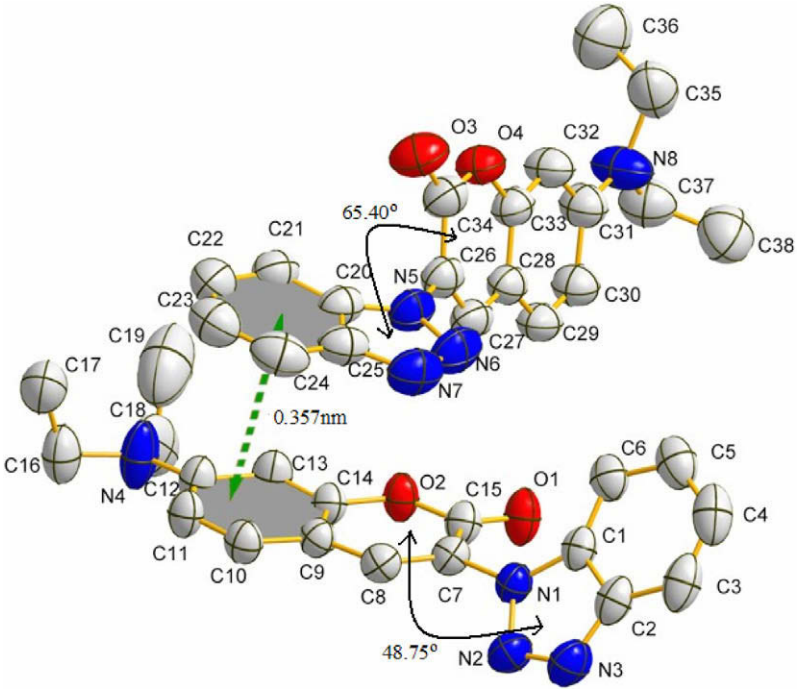

Fig. 1. Crystal structure of DABTC-1.

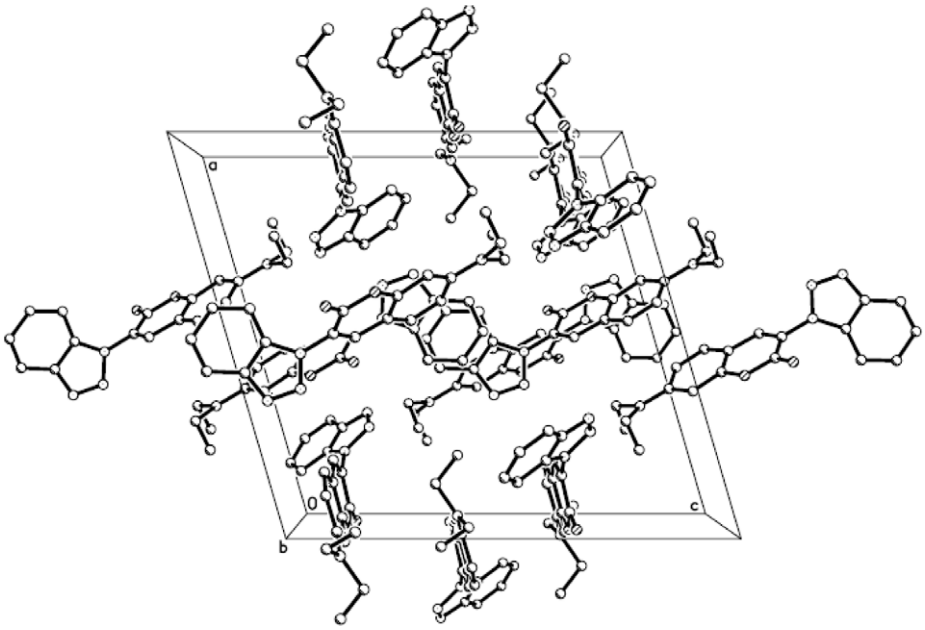

Fig. 2. Packing diagram of molecules of DABTC-1 along *a*-axis. H atoms are omitted for clarity.

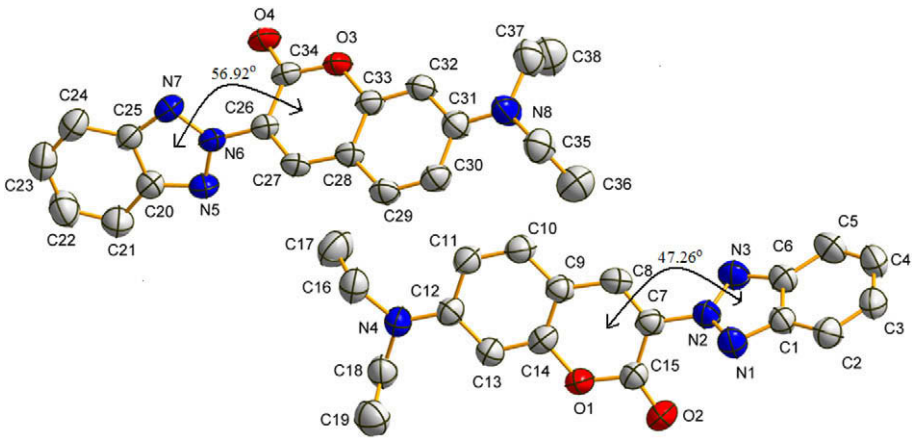

Fig. 3. Crystal structure of DABTC-2.

Acceptable crystals of DABTC-1 for X-ray analysis were obtained by slow evaporation of ethyl acetate solution, and the structure was measured by X-ray crystallography. The crystal of DABTC-1 belongs to the monoclinic space group $P2_1/c$, $a = 15.920(2)$ Å, $b = 12.8933(18)$ Å, $c = 17.083(3)$ Å, $\beta = 106.299(3)°$, $U = 3365.7(9)$ Å^3, $Z = 8$, $D_c = 1.320$ g cm^{-3}, $\mu = 0.089$ mm^{-1}. As shown in Fig. 1, there is an asymmetric unit consisted of two molecules in crystal structure of DABTC-1 due to the different space configuration of two ethylic groups of diethylamine in 7-position of coumarin ring. These two molecules are space conformers, the benzotriazole skeleton of one DABTC-1 molecule cross-paralleled and superposed with the coumarin ring of other DABTC-1 molecule, and the distance of the planes is about 3.6 Å. In addition, the benzotriazole skeletons are not coplanar with the coumarin rings in these two molecules, the dihedral angles are 65.40° and 48.75°, respectively.

The packing diagram for unit cell of DABTC-1 was shown in Fig. 2. There is cross ABAB-type stacking between the benzotriazole group of one DABTC-1 molecule and the coumarin ring of other DABTC-1 molecule, the interplanar (A···B) distance is approximately 3.6 Å, which means weak intermolecular π–π stacking interaction between DABTC-1 molecules in crystal lattice.

Acceptable crystals of DABTC-2 for X-ray analysis were also obtained by slow evaporation of ethyl acetate solution. The crystal of DABTC-2 belongs to the monoclinic space group $P2_1/c$, $a = 17.416(5)$ Å, $b = 12.743(4)$ Å, $c = 15.707(5)$ Å, $\beta = 102.527(5)°$, $U = 3403.1(18)$ Å^3, $Z = 8$, $D_c = 1.305$ g cm^{-3}, $\mu = 0.088$ mm^{-1}. Similarly, there is also an asymmetric unit consisted of two molecules in crystal structure of DABTC-2 due to the different space configuration of two ethylic groups of diethylamine in 7-position of coumarin ring (Fig. 3). Compared with DABTC-1, these

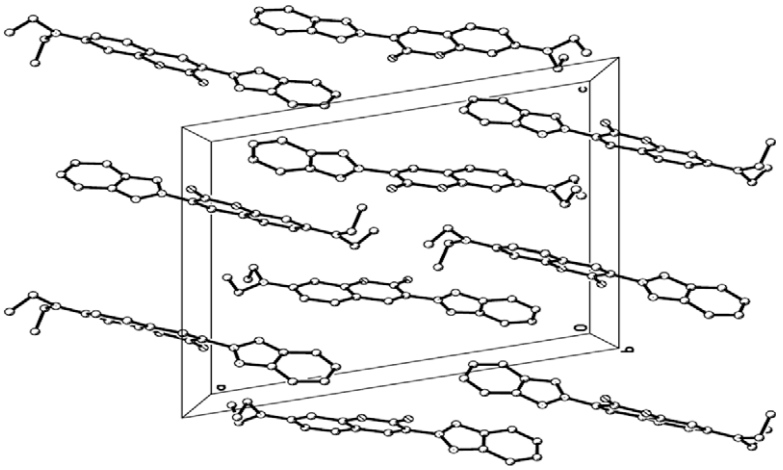

Fig. 4. Packing diagram of molecules of DABTC-2 along *c*-axis. H atoms are omitted for clarity.

space conformers did not neither parallel nor superpose each other. As shown in Fig. 4, there is no intermolecular π–π stacking interaction between DABTC-2 molecules in crystal lattice. From the crystal structure of DABTC-2, we can see that the benzotriazole skeletons are not also coplanar with the coumarin rings in these two molecules, the dihedral angles are 56.92° and 47.26°, respectively.

3.2. Absorption and fluorescence of DABTC-1 and DABTC-2

UV–vis absorption spectra of DABTC-1 and DABTC-2 in diluted chloroform solutions are given in Fig. 5. It is shown that the absorption spectrum of DABTC-1 exhibits absorptions at 253 nm and 414 nm, respectively. The absorption spectrum of DABTC-2 is similar to that of DABTC-1, there are two absorption at 253 nm and 424 nm. An important feature of the absorption spectrum of DABTC-2 is shown that the second absorption band at 424 nm was bathochromically shifted by about 10 nm with respect to that of DABTC-1 in which the second absorption band is at 414 nm, it can be generally deduced that the conjugative effect of the 2-substituted benzotriazole derivative (i.e. DABTC-2) is larger than that of the 1-benzotriazolyl isomer (i.e. DABTC-1).

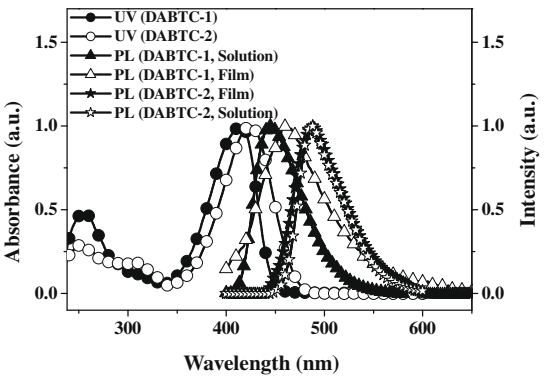

Fig. 5. UV–Vis absorption and photoluminescent spectra of the compounds in dilute chloroform solutions and the solid films.

Fig. 5 also shows the photoluminescent spectra of DABTC-1 and DABTC-2 in dilute chloroform solutions and the solid films. It is shown that DABTC-1 compound exhibits bright blue emission with peak at 447 nm and DABTC-2 compound exhibits bright blue–green emission at 485 nm in dilute solution, and the emission peak of DABTC-2 was red-shifted by about 38 nm compared with that of DABTC-1 due to the larger conjugation of molecule in DABTC-2. Compared with the emission spectra in the solutions, the emission peaks of the solid films of DABTC-1 and DABTC-2 are observed at 462 and 485 nm, respectively. The emission peak of DABTC-1 in the solid film was bathochromically shifted by 15 nm with respect to that in the solution, and much broader emission band of the solid film brought about the compact piling of the solids was occurred, suggesting that the compound in the solid film has more intermolecular interaction than that in solution situation, and thus may lead to change of the emission band. The emission spectrum of the film of DABTC-2 was similar to that of the solution, the emission peaks were at 485 nm, but the former was little broader than the latter. The differences between the films and the solutions were explained by the crystal structures of DABTC-1 and DABTC-2. There was weak intermolecular π–π stacking interaction between DABTC-1 molecules in crystal lattice, whereas no intermolecular π-π stacking interaction between DABTC-2 molecules existed in crystal lattice.

UV–vis absorption and photoluminescent spectra of coumarin 6 (C6) and 7 (C7) in diluted chloroform solutions show the maximum peaks at 456 nm (C6), 437 nm (C7), 490 nm (C6) and 491 nm (C7), respectively [25]. Compared with commercial coumarin 6 and 7, although the structure of DABTC-2 is similar to that of coumarin 6 and 7, UV–vis absorption and photoluminescent spectra of DABTC-2 shift to blue due to the electron-withdrawing benzotriazole substituents at 3-position.

The photoluminescence behaviors of DABTC-1 and DABTC-2 vs. the concentrations in chloroform solutions were shown in Fig. 6. It was found that the emission spectral features of DABTC-1 and DABTC-2 changed with the solution concentrations. The concentration required for

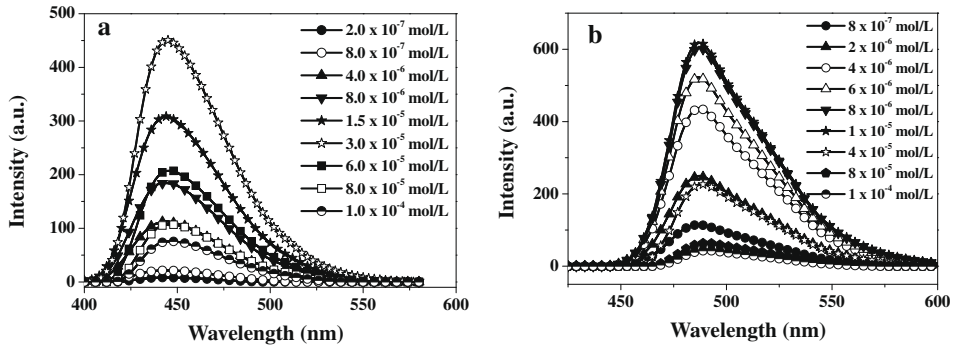

Fig. 6. The emission spectra of DABTC-1 (a) and DABTC-2 (b) in dilute chloroform solutions at room temperature.

the maximum emission intensity was different in DABTC-1 and DABTC-2, which implies that concentration plays an important role in the different dye molecules. There is the strongest blue emission at about concentration of 3.0×10^{-5} mol/L for DABTC-1 and 8.0×10^{-6} mol/L for DABTC-2, respectively. When the concentrations were lower than these concentrations, the relative emission intensities increased gradually with increasing the concentrations. When the concentrations were higher than these concentrations, the emission intensities were decreasing.

3.3. Fluorescence quantum yield of the compound **3** ($\Phi_{F,3}$)

Fluorescence quantum yields of DABTC-1 and DABTC-2 in chloroform solution were checked with anthracene, respectively. The quantum yield (Φ_F) were calculated according to the relationship [26,27]:

$$\Phi_F = \Phi_F^S \frac{\int_0^\infty I_F(\tilde{\nu})d\tilde{\nu}}{\int_0^\infty I_F^S(\tilde{\nu})d\tilde{\nu}} \left(\frac{1-10^{-A^S}}{1-10^{-A}}\right)\left(\frac{n}{n^S}\right)^2$$

where Φ_F^S is the quantum yield of anthracene as standard, which was assumed to be 0.25 for all environments [27]. The integral $\int_0^\infty I_F(\tilde{\nu})d\tilde{\nu}$ and $\int_0^\infty I_F^S(\tilde{\nu})d\tilde{\nu}$ are the areas under the emission curves of the investigated and standard compound, respectively. A and A^S are the absorbances at the wavelength of excitation, n and n^S are the refractive indices for the investigated and standard, respectively. In the research, the $\Phi_{F,\ DABTC\text{-}1}$ and $\Phi_{F,\ DABTC\text{-}2}$ are 0.53 and 0.69, respectively. Fluorescence quantum yields of Coumarin 6 ($\Phi_{F,\ Coumarin\ 6}$) in acetonitrile is 0.63 [28]. Fluorescence quantum yields of DABTC-1 and DABTC-2 are comparative to that of coumarin 6.

3.4. Quantum chemical calculations

From the crystal structures of DABTC-1 and DABTC-2 (Figs. 1 and 3), it was found that there were two molecules in the crystal structures. For the sake of quantum chemical calculations, we chose one molecule of them to optimize DABTC-1 and DABTC-2 geometrical structures, respectively. B3LYP/6-31G(d) optimized structures of DABTC-1 and DABTC-2 are close to their X-ray crystallographic data. The HOMO and LUMO levels of DABTC-1 and DABTC-2 were deduced using the DFT method as shown in Figs. S1 and S2, respectively. It can be seen that the levels of HOMO and LUMO of DABTC-1 were −5.510 eV and −1.589 eV, and the energy gap between HOMO and LUMO is about 3.921 eV. For DABTC-2, the data were −5.487 eV, −1.594 eV and 3.893 eV, respectively. It can be also found that the electron density distributions of the HOMO orbitals were different from that of the HOMO orbitals for DABTC-1 and DABTC-2.

The UV–vis absorption spectra of DABTC-1 and DABTC-2 were also calculated by the time-dependent density functional theory (TD-DFT) at the same level. The experimental and calculated data for the lower-lying singlet states of DABTC-1 and DABTC-2 were listed in Table 1. As shown in Table 1, there are some discrepancies between theoretical and experimental data due to several influencing factors, such as solvent effect and intermolecular interaction. It has been found that the lowest energy absorption at 414 nm for DABTC-1 or 424 nm for DABTC-2 was an excitation from the HOMO to the LUMO. The transition occurring at 253 nm was attributed to the electronic $\pi \rightarrow \pi^*$ transition from the HOMO to the LUMO+2 for DABTC-1 or from the HOMO−2 to the LUMO+1 for DABTC-2, respectively.

Table 1
Absorption spectra data of DABTC-1 and DABTC-2.

Compound	Transition character	OSC[a]	$\lambda_{max,\ cal.}$ (nm)	$\lambda_{max,\ exp.}$ (nm)[b]	Transition feature
DABTC-1	HOMO → LUMO	0.7397	369.32	414	$\pi \rightarrow \pi^*$
	HOMO → LUMO+2	0.1583	243.25	253	$\pi \rightarrow \pi^*$
DABTC-2	HOMO → LUMO	0.9473	378.24	424	$\pi \rightarrow \pi^*$
	HOMO−2 → LUMO+1	0.1778	233.37	253	$\pi \rightarrow \pi$

[a] Oscillator strength coefficients (f).
[b] λ_{max} in dichloromethane solvent.

3.5. OLED performance

The molecular structures of the materials and the devices with the configuration of ITO/2-TNATA (5 nm)/NPB (40 nm)/CBP: DABTC-1 or CBP: DABTC-2 (× wt%, 30 nm)/PBD (30 nm)/LiF (1 nm)/Al (100 nm) were depicted in Fig. 7. DABTC-1: CBP or DABTC-2: CBP was employed as the emitter, 2-TNATA, NPB, and PBD were used as hole injection, hole transport and electron transport materials, respectively. LiF was used as the electron–injection layer.

Fig. 8 shows the EL spectra of the devices with DABTC-1 and DABTC-2 doped at concentrations of 1.0 wt% at different driving voltages. The intensities of EL emissions increase gradually with increasing the driving voltages, but the emission spectral features do not change. The devices of DABTC-1 exhibit blue emissions with the maximum peaks at ca. 462 nm, the devices of DABTC-2 exhibit blue–green emissions with the maximum peaks at ca. 485 nm. The EL spectra of DABTC-1 and DABTC-2 are identical to the PL spectra of them in the solid films, respectively. Such results indicate that these emissions take place from DABTC-1 and DABTC-2 molecules.

Fig. 9 shows the representative luminance-current density–voltage characteristics of the devices doped DABTC-1 with different concentrations. At the doped concentration of 1.0 wt%, the device shows a turn-on voltage about 12 V, and the luminance reaches as high as 40 cd/m^2 at 21 V. At the doped concentration of 2.0 wt%, a turn-on voltage of the device is about 8.5 V, and the maximal luminance reaches 48 cd/m^2 at 15 V.

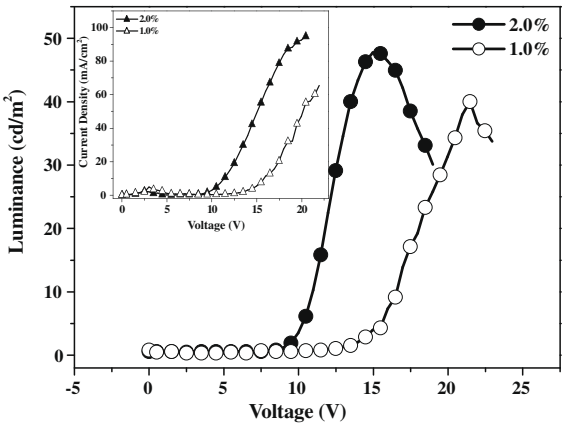

Fig. 9. The luminance vs. voltage and current density vs. voltage (inset) curves of the devices with different DABTC-1 concentrations.

Fig. 10 shows the representative luminance-current density–voltage characteristics of the devices doped DABTC-2 with different concentrations. The turn-on voltages of the devices at the doped concentrations of 1.0 wt% and 2.0 wt% were 10 V and 6 V, respectively. The maximal luminances were 371 cd/m^2 at 23 V for the device doped

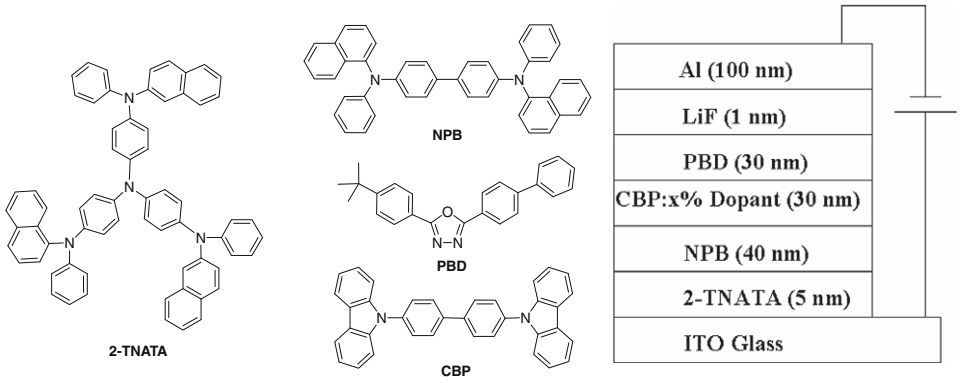

Fig. 7. The molecular structures of materials and the structure of EL devices.

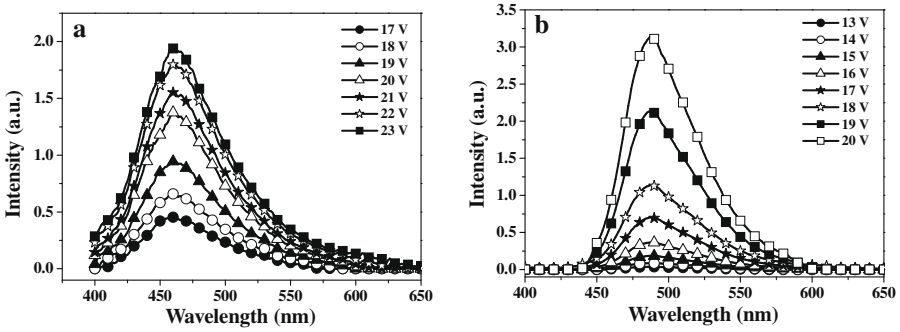

Fig. 8. EL spectra of the devices used DABTC-1 (a) and DABTC-2 (b) as dopants at different applied voltages. The devices with the configuration of ITO/2-TNATA (5 nm)/NPB (40 nm)/CBP: dopant (1.0 wt%, 30 nm)/PBD (30 nm) / LiF (1 nm)/Al (100 nm).

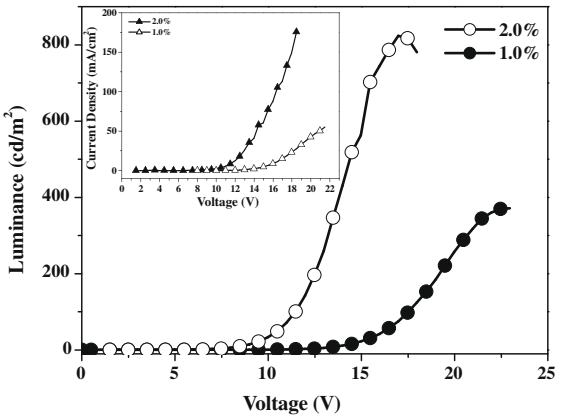

Fig. 10. The luminance vs. voltage and current density vs. voltage (inset) curves of the devices with different DABTC-2 concentrations.

concentration of 1.0 wt% and 823 cd/m^2 at 17 V for the device doped concentration of 2.0 wt%, respectively.

Fig. 11 shows the relationships between current efficiency and the current density in the devices with various DABTC-1 and DABTC-2 doping concentrations. It is shown that all doped devices have higher efficiencies at low current densities, and then the efficiencies fall off at higher current densities. The above finding indicates that the electron hole recombination may not be effective under high current density, revealing that the present host, CBP, might not be an optimal host material. The present device performance could be further improved by substituting other host candidates. Table 2 summarized the performances of the devices with various DABTC-1 and DABTC-2 doping concentrations in CBP host. It was shown that the 2 wt% DABTC-1 and DABTC-2 doped devices had better efficiencies.

It was interesting to note that the turn-on voltages of the devices decreased with the increasing of compounds (DABTC-1 or DABTC-2) doping concentration in the CBP host from Figs. 9 and 10. In view of the structures of the two compounds, they were substituted by the electron-withdrawing benzotriazoles regarded as accptors [29] and used as electron-transporting materials [30]. Furthermore, the host material CBP can provide good hole-transporting properties [31]. With DABTC concentration

Table 2
EL performances of DABTC-1 and DABTC-2 doped devices.

Compound		Maximum efficiency (cd/A)	Efficiency at 20 mA/cm^2 (cd/A)
DABTC-1	1.0 wt%	0.33 @ 0.22 mA/cm^2	0.09
	2.0 wt%	0.60 @ 0.10 mA/cm^2	0.15
DABTC-2	1.0 wt%	1.81 @ 0.16 mA/cm^2	0.97
	2.0 wt%	1.63 @ 0.40 mA/cm^2	1.05

increasing, the conductive characteristics of the devices was considerably improved, and the turn-on voltages of the devices were reduced. It was shown that benzotriazole group had excellent electron-transporting ability in these EL devices. From Figs. 9 and 10, it was found that the luminance of DABTC-2 devices was very stronger than that of DABTC-1 devices due to the larger conjugation of molecule in DABTC-2. Similarly, it was found that the current efficiency of DABTC-2 devices was higher than that of DABTC-1 devices (Fig. 11).

From above results, it was indicated that the performance of the DABTC-2 doped devices is be superior to that of the DABTC-1 doped devices.

3.6. Conclusions

We designed and prepared two new coumarin derivatives containing an electron-transporting moiety (benzotriazole), 7-*N*,*N*-diethylamino-3-(benzotriazol-1-yl)coumarin (DABTC-1) and 7-*N*,*N*-diethylamino-3-(benzotriazol-2-yl)coumarin (DABTC-2). The photoluminescent behaviors of the compounds in both solution and solid states were investigated and discussed. The doped devices fabricated from DABTC-1 or DABTC-2 doped in CBP show the EL spectra of DABTC-1 or DABTC-2 is identical to the PL spectra of them in the solid films, respectively. The ITO/2-TNATA (5 nm)/NPB (40 nm)/CBP: DABTC-1 (2.0 wt%, 30 nm)/PBD (30 nm)/LiF (1 nm)/Al (100 nm) device displayed the pure blue emission, a maximum luminous efficiency of 0.15 cd/A at the current density of 20 mA/cm^2, and maximum luminance of 48 cd/m^2 at 15 V. At the same condition, the DABTC-2 doped devices exhibited the brighter blue–green emission, a maximum luminous efficiency of 1.05 cd/A at the current density of 20 mA/cm^2, and maximum luminance of 823 cd/m^2 at 17 V.

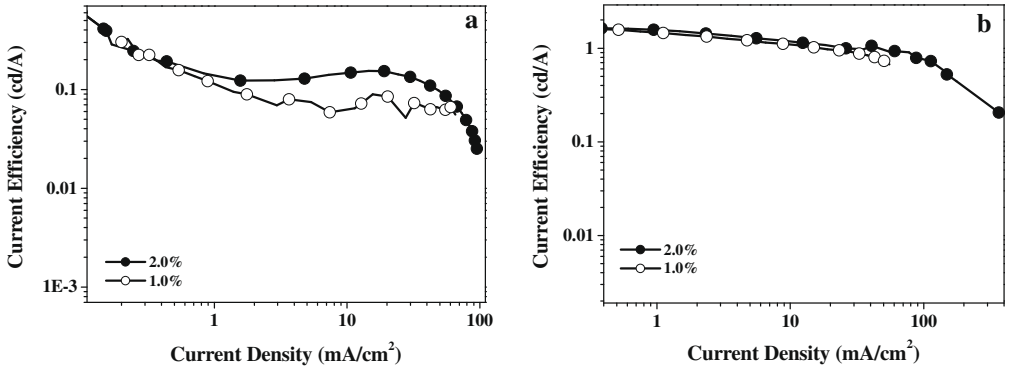

Fig. 11. Current efficiency-current density characteristics of the doped devices with various DABTC-1 (a) and DABTC-2 (b) concentrations.

Acknowledgements

This work was supported by the National Natural Science Foundation of China (Grant 60776006), the Program for Changjiang Scholars and Innovative Research Team in University (IRT0629) and also supported by 'Qing Lan' talent engineering funds (QL-05-23A) by Lanzhou Jiaotong University.

Appendix A. Supplementary material

The crystallographic data (excluding structure factors) of DABTC-1 and DABTC-2 had been deposited with the Cambridge Crystallographic Center as supplementary publication No. CCDC 733174 and No. CCDC 733173, respectively. Tables S1–S3 and Figs. S1 and S2 are given as supplementary information. Supplementary data associated with this article can be found, in the online version, at doi:10.1016/j.orgel.2009.09.023.

References

[1] C.W. Tang, S.A. VanSlyke, Appl. Phys. Lett. 51 (1987) 913–915.
[2] J.R. Sheats, H. Antoniadis, M. Hueschen, W. Leonard, J. Miller, R. Moon, D. Roitman, A. Stocking, Science 273 (1996) 884–888.
[3] R.H. Friend, R.W. Gymer, A.B. Holmes, J.H. Burroughes, R.N. Marks, C. Taliani, D.D.C. Bradley, D.A. Dos Santos, J.L. Bredas, M. LÖglund, M. LÖglund, W.R. Salaneck, Nature 397 (1999) 121–128.
[4] J. Shinar, R. Shinar, J. Phys. D: Appl. Phys. 41 (2008) 133001.
[5] K.C. Fylaktakidou, D.J. Hadjipavlou-Litina, K.E. Litinas, D.N. Nicolaides, Curr. Pharm. Des. 10 (2004) 3813.
[6] G. Jones, W.R. Jackson, C. Choi, W.R. Bergmark, J. Phys. Chem. 89 (1985) 294.
[7] T. Hiroshi, O. Yosho, I. Juzo, I. Masato, T. Atsushi, Jpn. Kokai Tokkyo Koho 1990 (1990) (CODEN: JKXXAF JP 02126241 A2 19900515 Heisei).
[8] H.E. Patel, K.R. Desai, J. Inst. Chem. 68 (1996) 78.
[9] D. Ray, P.K. Bharadwaj, Inorg. Chem. 7 (2008) 2252.
[10] S.R. Trenor, A.R. Shultz, B.J. Love, T.E. Long, Chem. Rev. 104 (2004) 3059.
[11] T.T. Hung, Y.J. Lu, W.Y. Liao, C.L. Huang, IEEE T. Magn. 2 (2007) 867.
[12] K. Hara, K. Sayama, Y. Ohga, A. Shinpo, S. Suga, H. Arakawa, Chem. Commun. (2001) 569.
[13] M. Fujiwara, N. Ishida, M. Satsuki, S. Suga, J. Photopolym. Sci. Technol. 2 (2002) 237.
[14] C.W. Tang, S.A. VanSlyke, C.H. Chen, J. Appl. Phys. 65 (1989) 3610.
[15] M. Mitsuya, T. Suzuki, T. Koyama, H. Shirai, Y. Taniguchi, Appl. Phys. Lett. 77 (2000) 3272.
[16] C.H. Chen, C.W. Tang, J.M. Shi, K.P. Klubek, US Patent 6020078, 2000.
[17] M.T. Lee, C.K. Yen, W.P. Yang, H.H. Chen, C.H. Liao, C.H. Tsai, C.H. Chen, Org. Lett. 8 (2004) 1241.
[18] J.L. Lai, J.S. Shiu, C.W. Kuo, US Patent 6727362 B1, 2004.
[19] T.Z. Yu, P. Zhang, Y.L. Zhao, H. Zhang, J. Meng, D.W. Fan, Org. Electron. 10 (2009) 653–660.
[20] B.B. Raju, T.S. Varadarajan, Laser Chem. 16 (1995) 109–120.
[21] J. Griffiths, V. Millar, G.S. Bahra, Dyes Pigments 28 (1995) 327–339.
[22] N. Kitamura, T. Fukagawa, S. Kohtani, S. Kitoh, K.-K. Kunimoto, R. Nakagaki, J. Photochem. Photobiol. A: Chem. 188 (2007) 378–386.
[23] T. Mori, K. Obata, K. Imaizumi, T. Mizutani, Appl. Phys. Lett. 69 (1996) 3309–3311.
[24] P. Sanna, A. Carta, M.E.R. Nikookar, Eur. J. Med. Chem. 35 (2000) 535–543.
[25] U.S. Raikar, C.G. Renuka, Y.F. Nadaf, B.G. Mulimani, A.M. Karguppikar, M.K. Soudagar, Spectrochim. Acta Part A 65 (2006) 673–677.
[26] K.A. Kozyra, J.R. Heldt, H.A. Diehl, J. Heldt, J. Photochem. Photobiol. A: Chem. 152 (2002) 199–205.
[27] M. Kaholek, P. Hrdlovič, J. Photochem. Photobiol. A: Chem. 127 (1999) 45–55.
[28] G. Jones II, W.R. Jackson, C. Choi, J. Phys. Chem. 89 (1985) 294–300.
[29] R. Lygaitisa, A. Matoliukstytea, N. Kreiveniene, J.V. Grazulevicius, J. Photochem. Photobiol. A: Chem. 167 (2004) 163–168.
[30] S.H. Ahn, M. Czae, E.R. Kim, H. Lee, S.H. Han, J. Noh, M. Hara, Macromolecules 34 (2001) 2522–2527.
[31] H. Kanai, S. Ichinosawa, Y. Sato, Synth. Met. 91 (1997) 195–196.